Controlled covalent functionalization of a graphene-channel of a field effect transistor as an ideal platform for (bio)sensing applications

Vladyslav Mishyn, Teresa Rodrigues, Yann R. Leroux, Patrik Aspermair, Henri Happy, Johannes Bintinger, Christoph Kleber, Rabah Boukherroub, Wolfgang Knoll, Sabine Szunerits

Controlled Covalent Functionalization of Graphene-Channel of a Field Effect Transistor as Ideal Platform for (Bio)sensing Applications

Vladyslav Mishyn,[1] Teresa Rodrigues,[1,2] Yann R. Leroux,[3]* Patrik Aspermair,[2] Henri Happy,1 Johannes Bintinger, [2] Christoph Kleber,[4] Rabah Boukherroub,[1] Wolfgang Knoll,[2,4]* and *Sabine Szunerits*[1]*

[1]*Univ. Lille, CNRS, Centrale Lille, Univ. Polytechnique Hauts-de-France, UMR 8520 - IEMN, F-59000 Lille, France*

[2] *Biosensor Technologies, AIT Austrian Institute of Technology GmbH, 3430 Tulln, Austria*

[3] *Univ. Rennes, CNRS, ISCR – UMR 6226, Campus de Beaulieu, F-35000 Rennes, France.*

[4] *Department of Physics and Chemistry of Materials, Faculty of Medicine/Dental Medicine, Danube Private university, Krems, Austria.*

Abstract:

The controlled covalent functionalization of the graphene channel of a field effect transistor, based on interdigitated gold electrodes (source and drain), via electrochemical grafting, using specifically designed aryl diazonium species is demonstrated to allow the simple fabrication of a general platform for (bio)sensing applications. The electrochemical grafting of a protected ethynylphenyl diazonium salt leads to the deposition of only a monolayer on the graphene channel. This controlled covalent functionalization of the graphene channel results in a charge mobility of the GFET of 1739±376 $cm^2V^{-1}s^{-1}$ and 1698±536 $cm^2V^{-1}s^{-1}$ for the holes and electrons, respectively, allowing their utilization as (bio)sensors. After deprotection, a dense and compact ethynylphenyl monolayer is obtained and allows the immobilization of a wide range of (bio)molecules by Click Chemistry coupling reaction (Huisgen 1,3-dipolar cycloaddition). This finding opens promising options for graphene-based (bio)sensing applications.

Keywords: graphene, field effect transistor, diazonium chemistry, biosensing

*To whom correspondence should be send to: wolfgang.knoll@dp-uni.ac.at or sabine.szunerits@univ-lille.fr (SS)

1. Introduction

Graphene-based field effect transistors (GFETs) stand out for their small size, excellent electrical characteristics and high sensitivity to surface charges and electrical fields, making them ideal components for future electronics and electrical transducers for diagnostics.[1] The tuning of the electrical properties of GFETs remains an important research focus as it has important implications on the sensitivity of electrical biosensors.[2] To this end, graphene non-covalent [3] and covalent [4, 5] functionalization strategies have been described in the literature since the pioneer works of the Manchester group in 2004.[6] Physisorption of alkaline metal atoms and gas molecules has been shown to alter the conductivity of graphene, shift its neutrality point (Dirac point) and affect the mobilities of the charge carriers.[7] Non-covalent functionalization of graphene through π-π interactions, such as by the use of pyrene derivatives as anchoring groups, has also shown to be an effective method to dope GFETs.[8] These non-covalent graphene functionalization strategies have the merit of fully preserving the graphene lattice aromaticity and electrical performance.[9] While these interactions are rather strong, non-covalent approaches are expected to be less compatible with long term use of GFETs.[10, 11] To obtain stable and robust surfaces, chemical functionalization via covalent grafting is by far the most promising approach, and widely considered as an essential step for the construction of robust chemical and biological sensors.[12-14] Covalent surface grafting of graphene via diazonium chemistry is largely employed.[4, 12, 13, 15-17] The availability of diazonium salts bearing different functional groups makes this approach highly versatile. Generally, this grafting method is based on a transfer of an electron from graphene to the aryl diazonium cation, forming an aryl radical after loss of N_2 (**Figure 1a**). Then, this radical reacts with the graphene network to form a covalent bond with one of the carbon atoms. This results in changing the carbon hybridization from sp^2 to sp^3 and displacing it out of the graphene plane by about 0.7 Å.[18] Spontaneous aryl diazonium grafting has been shown to mainly proceed on graphene edges and defects.[19-22] In the case of electrochemically induced aryl diazonium grafting, the approach is effective on both the graphene basal plane and its edges, resulting generally in higher surface loading of functional groups.[17]

Even though this surface chemistry approach has been widely employed, the bottleneck to overcome with covalent attachment strategies using diazonium chemistry is to preserve the conductivity of the graphene sheet and its charge mobility. In the case of 4-nitrobenzene diazonium tetrafluoroborate salt, which is by far the most studied aryl diazonium derivative, in most cases [17, 23-25] a decrease in graphene conductivity occurs with increasing the grafting time (spontaneous grafting) due to the increased sp^2/sp^3 transitions. The electron-withdrawing

properties of the nitro group lead to a clear positive shift in Dirac point, resulting in a hole doping. Only a few other aryl diazonium salts have been studied for graphene functionalization, [26-29] but led to similar observations related to Dirac point shifts and a decrease of conductivity. Very recently, Pagliara and coworkers demonstrated that the electronic structure of graphene can be preserved even after covalent modification by using specifically designed 3,4,5-trimethoxybenzene diazonium salts.[13] While this finding is against the possibility to open a band gap in graphene by covalent functionalization and thus the use of graphene in electronic applications, this argues in favor of using graphene as sensing channel in transistors.

Here we demonstrate that CVD-grown graphene covalently modify with a monolayer of phenylacetylene, represents an ideal surface chemistry approach for GFET (**Figure 1a**). Electrochemical reduction of 4-(triisopropylsilyl)ethynyl]benzene diazonium tetrafluoroborate (TIPS-Eth-ArN_2^+) and further chemical deprotection of the triisopropylsilyl group results in a graphene modified interface with charge mobility above 1000 $cm^2V^{-1}s^{-1}$. This process is not only highly reproducible, but also the anchoring of alkynyl functional groups to the graphene transducer allows for further covalent immobilization of a wide range of molecules in a surface orientated manner using Cu(I) based "click" chemistry reaction. [30, 31]

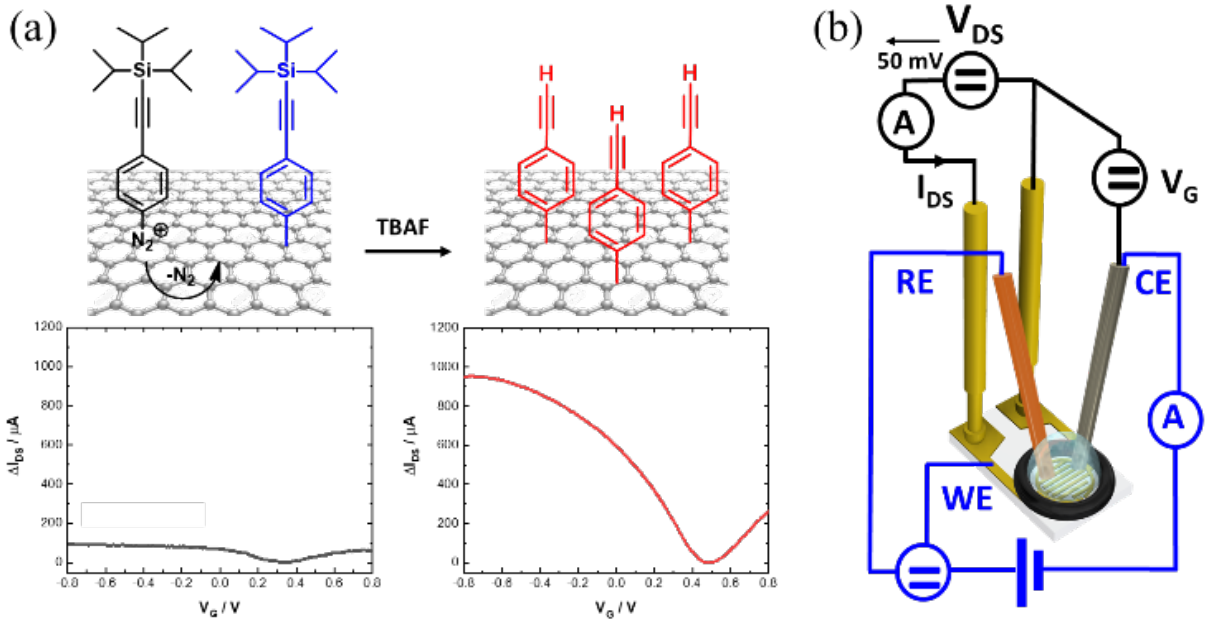

Figure 1. (a) Electrochemically driven anchoring of 4-[(triisopropylsilyl)ethylenyl]benzene diazonium tetrafluoroborate diazonium salt, followed by chemical deprotection forming alkynyl-terminated GFET devices. $I_{DS}V_G$ curve of GFET before (black) and after modification and deprotection (red). (b) Scheme of the liquid gated GFET device allowing for electrical measurements as well as electrochemical surface modifications to be performed.

2. Results and discussions.

2.1. Characterization of GFET formed on interdigitated electrodes

In this work, the investigated GFET devices are based on graphene coated interdigitated gold electrodes (IDE) with a layout consisting of 90 pair electrodes, each with a width of 10 µm, separated by 10 µm (**Figure 2a**) and arranged in an array of 3.5 mm in diameter. The monolayer graphene used in this work is grown by chemical vapor deposition (CVD) on commercial Cu foil. Transfer of graphene onto the IDE was achieved by coating graphene with polymethylmethacrylate (PMMA), a polymer supporting layer, to prevent graphene from collapsing. The wet transfer comprises several steps, (see **Scheme S1**) and uses a slow rate Cu etchant that avoids degradation of graphene. Recording a SEM image of the graphene coated IDE (**Figure 2a**) validates the complete coverage of the drain-source channel with graphene sheets with the quality of a monolayer graphene, as seen from the Raman spectrum (**Figure 2b**).

The Raman spectrum of CVD graphene consists of three main peaks at 1350, 1580 and 2706 cm^{-1} attributed as D (defects in the graphene sheet), G (graphene sp^2 carbon) and 2D (secondary D band) peaks, respectively. The low-intensity D+D'' contribution at ~2450 cm^{-1} appears due to a combination between D and the D'' peak at ~1100 cm^{-1} (not shown). The intensity ratio between 2D and G bands is 2.04. Generally, a 2D/G intensity ratio higher than 2 suggests that graphene monolayer has low charge impurities and proves the high-quality of the graphene monolayer deposited onto the surface of the device.[32] The intensity ratio between D and G peaks is 0.35 in the graphene lattice after transfer, indicating a low disorder. In order to examine the uniformity of the graphene film, a Raman mapping over 20×20 μm^2 area was explored. Most of the scanned area has a signature of $I_{2D}/I_G > 2$ and $I_D/I_G < 0.35$ which further confirms the uniform coverage of high-quality monolayer graphene (**Figure S1**).

From the AFM image in **Figure 2c**, a surface roughness of about 1 nm is observed, consistent with the deposition of a single graphene layer.[33]

The low surface roughness is in line with an efficient removal of the PMMA protection layer by first exposing the film to UV/ozone, followed by hot acetone washing for 30 min (**Figure 2d**). XPS analysis of the C1s core level spectrum is dominated by the band at a binding energy BE = 284.7 eV ascribed to the C-sp^2. Additional bands at BE = 285.0, 286.4 and 288.6 eV are due respectively to C-sp^3 components mostly present at the grain boundaries of the large graphene sheets, and edge functions such as C-O and C=O (**Figure 2e**).

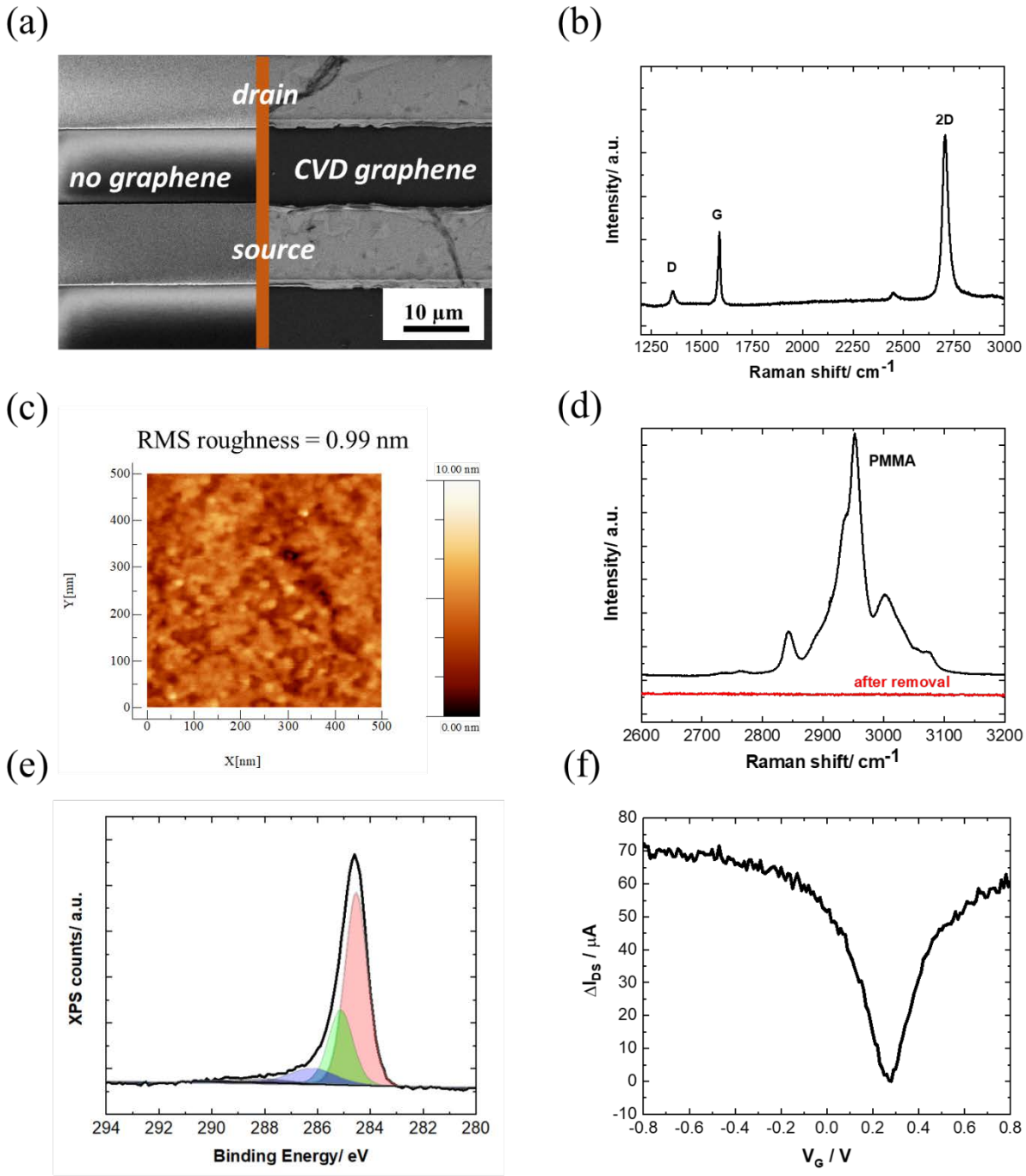

Figure 2. Characterization of the unmodified GFET: (a) SEM image of the IDE chip and after coating with CVD graphene showing full coverage of the drain-source channel. (b) Raman spectrum and (c) AFM image of the graphene channel. (d) Raman spectrum of PMMA coating before and after exposing the graphene/PMMA film to UV/ozone followed by hot acetone washing for 30 min. (e) C1s core level spectrum of the graphene channel. (f) IDSVG curve of IDE coated with graphene in PBS 1× (equal to $I_{DS}V_G$ curve in Figure 1a, but different scale).

The transfer characteristics of the GFET as a function of the gate voltage (V_G) is seen in **Figure 2f**. The Dirac point, which corresponds to the charge neutrality point is found at approximately 0.3 V vs. Ag/AgCl. The field-effect mobility, μ_{ef}, is obtained from the linear part of the transfer characteristics positive and negative to the Dirac point, using the following equation:

$$\mu_{ef} = \frac{dI_{DS}}{dV_G} \times \frac{L}{WV_{DS}C_{EDL}} \quad (1)$$

where L and W are the channel length and width (1.00 x 10^{-5} m and 4.90 x 10^{-1} m, respectively), V_{DS} is the source–drain voltage (V_{DS} = 50 mV), and C_{EDL} the electrical double layer capacitance extracted from the leakage current (**Figure S2**). Prior to the modification treatment, the calculated anodic hole mobility, μ_h, and cathodic electron mobility, μ_e, are 335±70 and 318±80 $cm^2V^{-1}s^{-1}$, respectively. These values are rather low compared to the extraordinary intrinsic high charge mobility limit of graphene of 200 000 $cm^2V^{-1}s^{-1}$. [34, 35] This can be explained by two different phenomena: first, it is now well-known that the choice of the surface where graphene is deposited is of utmost importance. For instance, SiO_2 surfaces tend to trap charges and impurities which can decrease graphene mobility by at least one order of magnitude. [36, 37] Here, gold as IDE on glass has been chosen as substrate and may impact drastically graphene mobility; second, it is also well-known that a complete removal of the polymer supporting layer (here PMMA) residuals is a problematic issue, even after a long period of exposure to acetone.[38] And even if great care has been taken here, such residuals have also a huge impact on the measured graphene mobility. Interestingly, Bouilly and coworkers [39] recently reviewed GFET as bioanalytical sensors. Whereas it is often assumed that high quality and high mobility of the graphene channel on the GFET is a required condition to obtain efficient sensors with low limit of detection (LOD), they observed that there is no significant correlation between graphene quality (mobility) and LOD values. Indeed, from the data collected for this review, reported mobility values as low as 200 $cm^2V^{-1}s^{-1}$ for exfoliated graphene [40] or 6 $cm^2V^{-1}s^{-1}$ for reduced graphene oxide (rGO) [41] allowed very low LOD (~fM or lower) in proteins sensors. Hence, the measured graphene mobility above 200 $cm^2V^{-1}s^{-1}$ in our case should allow the fabrication of efficient (bio)sensors in a simple way using commercially available IDE substrates without the need for lithography techniques.

2.2. Electrochemical surface grafting of TIPS-Eth-ArN_2^+ on the GFET

Several works reported on efficient graphene functionalization under electrochemical control. It was noted that the application of an electrochemical potential shifts the Fermi level of graphene,[17] increasing the probability for a direct attack of the covalent sp^2 bonds. We thus opted for the electrochemical grafting of a triisopropylsilyl protected ethynylphenyl diazonium

salt (**Figure 1a**), 4-[(triisopropylsilyl)ethynyl]benzene diazonium tetrafluoroborate (TIPS-Eth-ArN_2^+), known for its surface limiting grafting capabilities due to the presence of the bulky triisopropylsilyl (TIPS) group.[42, 43] For this purpose, cyclic voltammetry was applied as a powerful technique able to monitor *in situ* electron-transfer processes during the electrochemical reactions. The graphene channel of the GFET was used as working electrode thanks to the liquid gated configuration of our system (**Figure 1b**). A broad monoelectronic cathodic peak is observed at -0.2 V (vs. Ag/AgCl) by scanning the potential from +0.3 V to -0.6 V (vs. Ag/AgCl) at a scan rate of 50 mVs^{-1}. (**Figure 3a**) There is no anodic peak associated with the cathodic one, corresponding to the cleavage of N_2 groups coupled to the formation of aryl radicals. The electrochemical reduction current of TIPS-Eth-ArN_2^+ at -0.2 V decreases already after the first cycle, indicating that graphene channel is blocked by the deposition of an insulating organic film and thus the successful surface functionalization of this latter (**Figure 3a**). The success of the surface grafting was additionally validated by XPS analysis (**Figure 3b**). The change in the C1s core level of 4-(tri(isopropyl)silyl)ethynylphenyl (TIPS-Eth-Ar) modified GFET (**Figure 3b**) compared to unmodified GFET (**Figure 2e**) is in line with a change in the chemical environment after graphene functionalization. Furthermore, after TIPS-Eth-ArN_2^+ grafting, the presence of the bulky TIPS groups is confirmed by the presence of Si-C band at 283.7 eV and an increase in the intensity of the C-sp^2 component is ascribed to the contribution of C-sp^2 signal from the carbon atoms of the phenyl rings of the diazonium salt. The highly reactive nature of aryl radicals results, in most cases, in the formation of disordered polyaryl layers, which in the case of field effect transistors will reduce the dynamic range of sensing as it might be as thick as the Debye screening length, not being the case while using the bulky TIPS-Eth-ArN_2^+ precursor which limits the surface modification to a functional monolayer.[42, 43] Indeed, grafting of TIPS protected diazonium salt is a self-inhibited process and a full monolayer coverage is reached even after one cycle independent on the concentration of the diazonium salt used (1, 5 and 10 mM). This indicates that ligand density cannot be varied. An increase in surface roughness to 1.87 nm was determined by AFM measurements (**Figure 3c**). With a theoretical height of 4-[(triisopropylsilyl)ethynyl]benzene of 1.01 nm,[42] the coating thickness is in agreement with a controlled surface grafting of the 4-[(triisopropylsilyl)ethynyl]benzene radical on graphene and the prevention of the formation of multilayer branched structures, as observed in other works.[16] The success of the integration of TIPS-Eth-Ar onto graphene in one scan is further evident by the cyclic voltammograms of ferrocenemethanol (1 mM/PBS 1×) on unmodified GFET and GFET modified by TIPS-Eth-Ar (GFET-TIPS) (**Figure 3d**). Whereas a reversible oxidation is detected onto unmodified GFET,

a complete blocking of the electron transfer from ferrocenemethanol to GFET-TIPS is observed. Comparison of the Raman spectra of transferred CVD graphene before (**Figure 2b**) and after electrografting (**Figure 3e**) of TIPS-Eth-ArN_2^+ indicates an increase in the ratio between D and G band intensity. The D peak arises from the defect-involved double resonant Raman process at the K point in the Brillouin zone [44] and is attributed to the transition from sp^2 to sp^3 hybridization of the graphene carbon atoms. It is an indication of the degree of covalent modification of graphene and as expected the I_D/I_G ratio increased from 0.35 (GFET) to 0.67 (GFET-TIPS), which demonstrates an increase in the disorder in the graphene lattice due to the covalent modification.

Interestingly, electrografting of aryl diazonium salts results in strongly improved $I_{DS}V_G$ curve characteristics (**Figure 3f**) with slopes as steep as ~ 1750 µA/V. The process proved in addition to be highly reproducible (**Figure S3b**) with hole mobility, μ_h, and electron mobility, μ_e, of 1739±376 $cm^2\ V^{-1}\ s^{-1}$ and 1698±536 $cm^2\ V^{-1}\ s^{-1}$, respectively as determined on 10 different devices. Furthermore, the stability of the TIPS modified GFET devices evaluated 1 month after having been stored in the dark at room temperature is remarkably maintained, being observed just a slight decay on the drain-source current, but a negligible shift of the Dirac point (**Figure S3b**). As such, graphene p-doping produced by the grafting of TIPS-protected diazonium does not change overtime.

This observation is contradictory with a covalent functionalization implying an increase of the number of carbon atoms hybridization from sp^2 to sp^3 leading to a decrease of graphene charge mobility. Ago *et al.* [45] already reported that short exposures to aryl diazonium can have a positive effect by removing polymer residuals present on the surface of graphene samples which can explain in our case the improved conductivity of the GFET-TIPS channel. These values of charge mobilities have to be compared with the one found in the literature. In the majority of the examples, covalent functionalization of graphene has been performed using spontaneous grafting. As mentioned above, using spontaneous grafting, covalent functionalization is favored on the edges and defects of graphene materials[19-22] and lead to lower surface coverage than electrochemically induced aryl diazonium grafting. Whereas spontaneous grafting often leads to graphene charge mobility below 600 $cm^2V^{-1}s^{-1}$, [23, 29, 46, 47] when considering electrochemically driven aryl diazonium reduction this value decreases down to 10 $cm^2V^{-1}s^{-1}$.[17] Such mobility value above 1000 $cm^2V^{-1}s^{-1}$ is unprecedented and can be explain by the control surface functionalization of the graphene channel by using specifically designed sterically hindered aryl diazonium salts allowing the covalent attachment of only a monolayer.

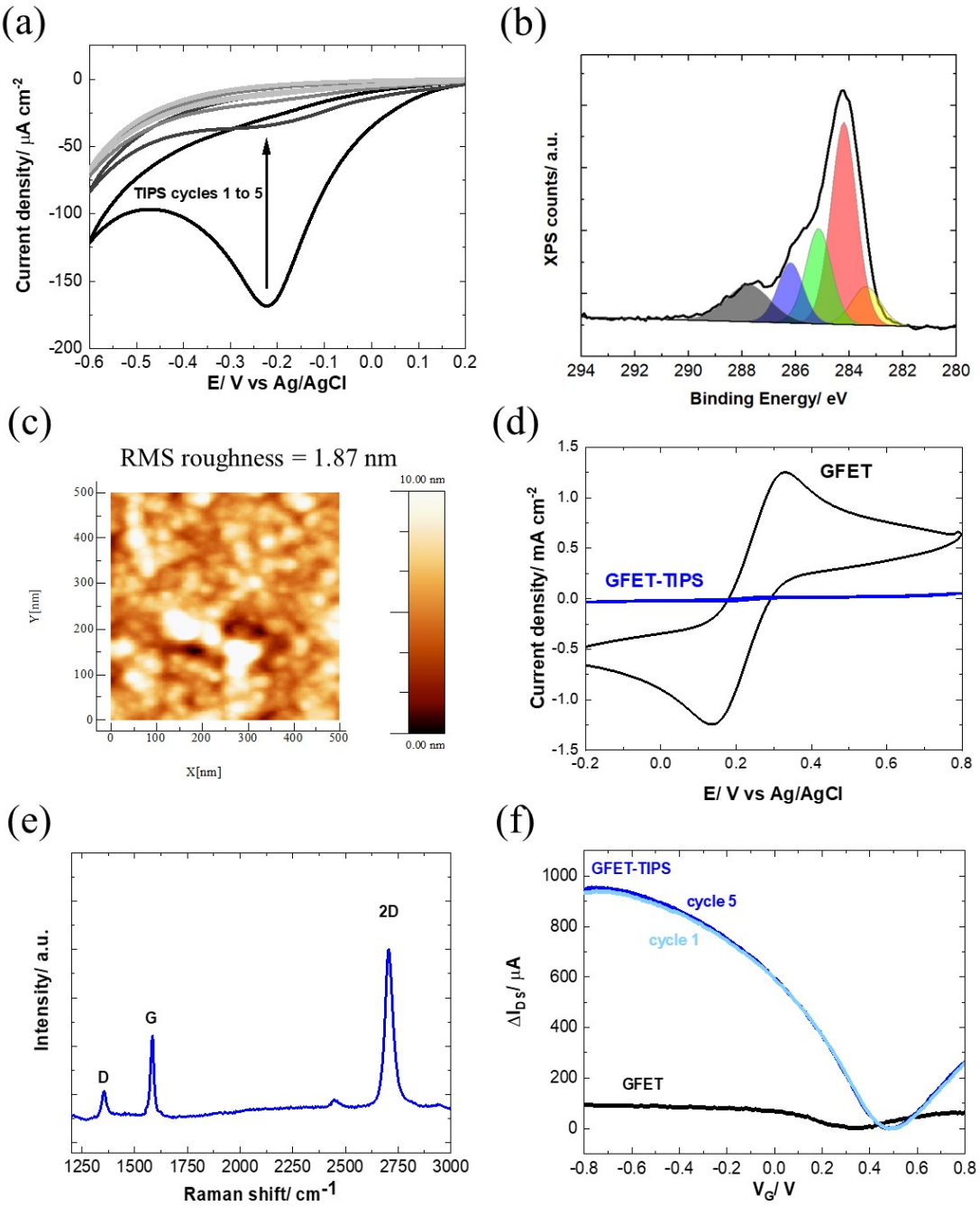

Figure 3. Characterization of the GFET-TIPS: (a) Electrochemical reduction of a solution of TIPS-Eth-ArN_2^+ (10 mM) in 0.1 M *n*-tetrabutylammonium hexafluorophosphate (nBu_4PF_6) in acetonitrile via cycling between +0.2 V and -0.6 V (vs. Ag/AgCl) at a scan rate of 50 mVs^{-1}. The reduction peak is visible at approximately -0.2 V vs. Ag/AgCl. (b) C1s core level spectrum and (c) AFM image of the GFET-TIPS channel. (d) Cyclic voltammograms of ferrocenemethanol (1mM/PBS 1×) on GFET and GFET-TIPS, scan rate 100 mVs^{-1}. (e) Raman spectrum of GFET-TIPS. (f) Transfer characteristics of GFET before (black) and after modification with TIPS-Eth-ArN_2^+ (blue) for several cycles. The $I_{DS}V_G$ of GFET before (black) is the same as illustrated in Fig 1(a) and integrate to allow easier comparison.

Modification of the electronic properties of the graphene channel is achieve during the first cycle. The following cycles do not alter the overall behavior. The Dirac point shifted from +0.3 V (vs. Ag/AgCl) to +0.5 V (vs. Ag/AgCl) for GFET-TIPS. In control experiments, GFETs were cycled between +0.2 V and -0.6 V (vs. Ag/AgCl) in an acetonitrile solution containing only 0.1 M *n*-tetrabutylammonium hexafluorophosphate salt (NBu_4PF_6) as supporting electrolyte, in the absence of diazonium salt. The transfer characteristic remained the same, ruling out any electrochemical doping (**Figure 4a**).

The change of the Dirac point to more positive values is in line with *p*-doping effect of the latter one. This has been also observed by others for GFETs functionalized with 4-nitrobenzene diazonium salt.[23, 48] To understand the mechanism behind the transfer characteristics a scatter plot of the peak position of the 2D band (ω_{2D}) vs. the position of the G Raman band (ω_G) was constructed by extracting the parameters from Raman mapping experiments of a GFET-TIPS interface (**Figure S4**. To distinguish between n- and p-doping the trend from literature data of mechanically exfoliated monolayer graphene doped by electrostatic gating is included.[49] The initial GFET device lies in the very low doped region, while after functionalization, graphene is shifted along the p-doped branch. The density of the reacted sites σ, quantitatively correlated with I_D/I_G ratios, was extracted using the correlation defined by Lucchese et al: [50]

$$\frac{I_D}{I_G} = C_A \frac{r_A^2 - r_S^2}{r_A^2 - 2r_S^2}\left[\exp\left(-\frac{\pi r_S^2}{L_D^2}\right) - \exp\left(-\frac{\pi(r_A^2 - r_S^2)}{L_D^2}\right)\right] + C_S\left[1 - \exp\left(-\frac{\pi r_S^2}{L_D^2}\right)\right] \qquad (2)$$

With L_D being the distance between defects, r_s and r_A the structurally demanded region around each defect site and activated region. Using r_s =0.07 nm and and r_A=1.0 nm[48], C_S and C_A values of 0.86 and 4.56, respectively[50] and the I_D/I_G ratios determined by Raman mapping (**Figure S4**), the surface defect site σ (σ =$1/L_D^2$) for graphene was estimated as $3.6\pm1.3\times10^{12}$ cm^{-2} being lower than the estimated saturation of 1×10^{15} cm^{-2}.[15]

We performed the same experiment with 4-nitrobenzene diazonium tetrafluoroborate (**Figure 4b**) as well with some other diazonium salts (**Figure S5**). In all cases, the same phenomenon was observed as with TIPS-Eth-ArN_2^+: an increase in mobility after the first cycle, decreasing however with consecutives scans due to the formation of multilayered branched structures (**Figure 4c**). The final charge mobilities of the different GFET modified interfaces (**Table S1**) were all less compared to that recorded on the GFET modified with TIPS-Eth-ArN_2^+ diazonium salt. Finally, GFET-TIPS channels have a decreased resistivity compared to GFET alone, which is almost independent of gate voltage applied (**Figure 4d**). Such behavior has also been

observed by Gao *et al.* considering graphene covalently functionalized by 4-nitrobenzene diazonium salts. [46] **Table S1** lists the graphene mobility values related to the other aryl diazonium salts that we use for comparison and are in line with our findings.

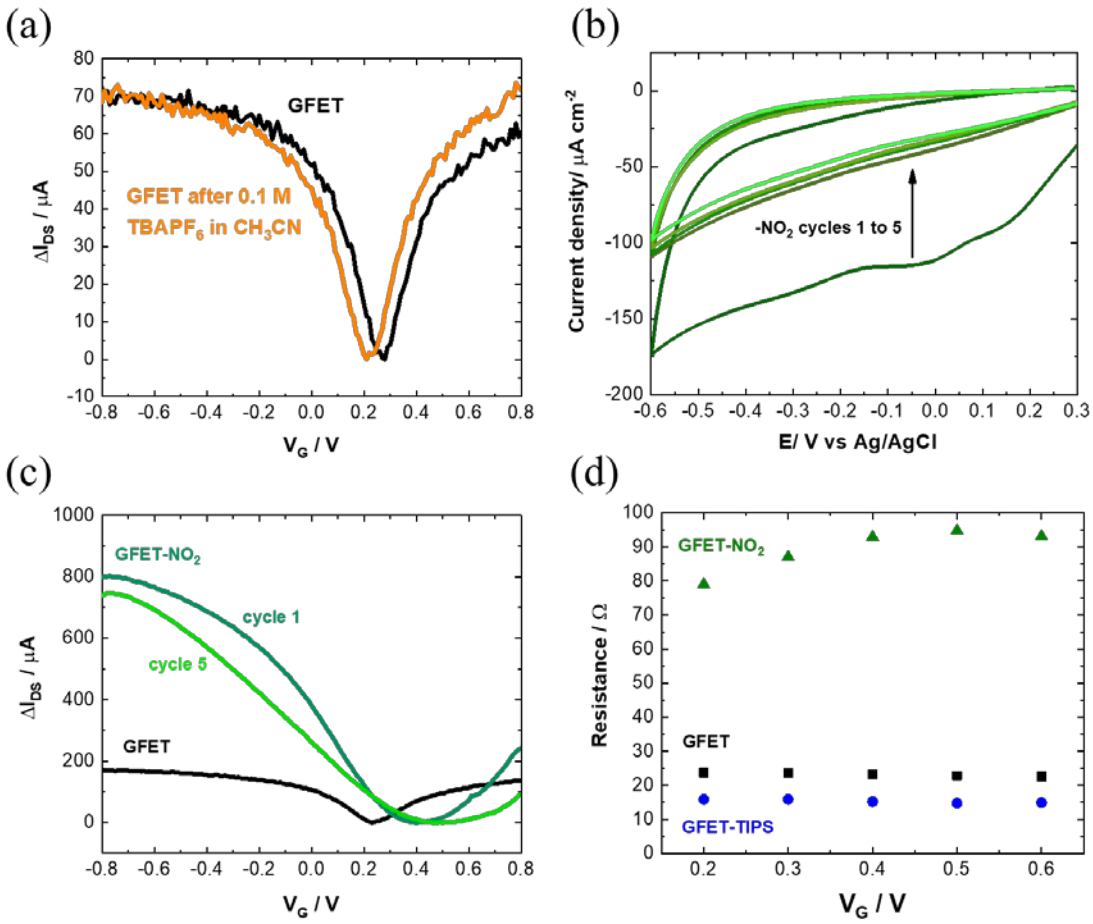

Figure 4. Control experiments: (a) $I_{DS}V_G$ of GFET before (black) and after (orange) electrochemical cycling a scan rate of 50 mVs^{-1} in 0.1 M *n*-tetrabutylammonium hexafluorophosphate (nBu_4PF_6) in acetonitrile. (b) Electrochemical reduction of a solution of 4-nitrobenzene diazonium tetrafluoroborate (10 mM) in 0.1 M nBu_4PF_6 in acetonitrile via cycling between +0.3 V and -0.6 V (vs. Ag/AgCl) at a scan rate of 50 mVs^{-1}. The reduction peak is visible at approximately -0.05 V vs. Ag/AgCl. (c) $I_{DS}V_G$ of GFET-NO_2 after 1 and 5 cycles as compared to pristine GFET. (d) Variation of resistivity with applied V_G for GFET (black), GFET-TIPS (blue) and GFET-NO_2 (green).

2.3. TIPS Deprotection and Click Chemistry

In order to have access to the alkynyl groups, a deprotection step is mandatory. Stable and highly reproducible ethynyl-terminated graphene channels were formed via the electro-

chemical reduction of TIPS-Eth-ArN_2^+ followed by chemical deprotection of the TIPS group with tetrabutylammonium fluoride (TBAF) solution. (**Figure 5a**) Chemical deprotection of the TIPS group with TBAF does not alter the transfer characteristics of the GFET as a function of gate voltage, V_G. (**Figure 5b**) The Dirac point (**Figure 5b**) shifted from +0.5 V back to +0.3 V after removal of the TIPS groups. Indeed, the formed ethynyl-terminated graphene channels with no particular electron donating or withdrawing group did not cause any obvious change in neither the *n* nor *p* type doping of the graphene. The presence of fluoride ions also did not modify the conductivity level of graphene. This is in line with Raman image of ethynyl-terminated chips (**Figure 5c**), with comparable I_D/I_G ratio as for GFET-TIPS (**Figure 3e**), confirming that the chemical treatment of the surface with TBAF only removed the TIPS groups without affecting the graphene lattice. Lucchese et al.[51] reported an adapted simple formula allowing a rough estimation of the distance between attached aryl groups, La, from the I_D/I_G ratio, where $(1/La)^2 \sim I_D/I_G$. From this formula, after electrografting, we estimated La to be ~ 1.5 nm corresponding to a surface coverage $\Gamma \sim 10^{-10}$ mol cm^{-2}. The deprotected substrate was further treated by "click" chemistry reaction (Huisgen 1,3-dipolar cycloaddition [30, 31]) using azidomethylferrocene. (**Figure 5a**) The success of the incorporation of ferrocene units onto the

GFET is seen from the presence of the Fe2p component in the XPS survey spectrum. (**Figure 5d**)

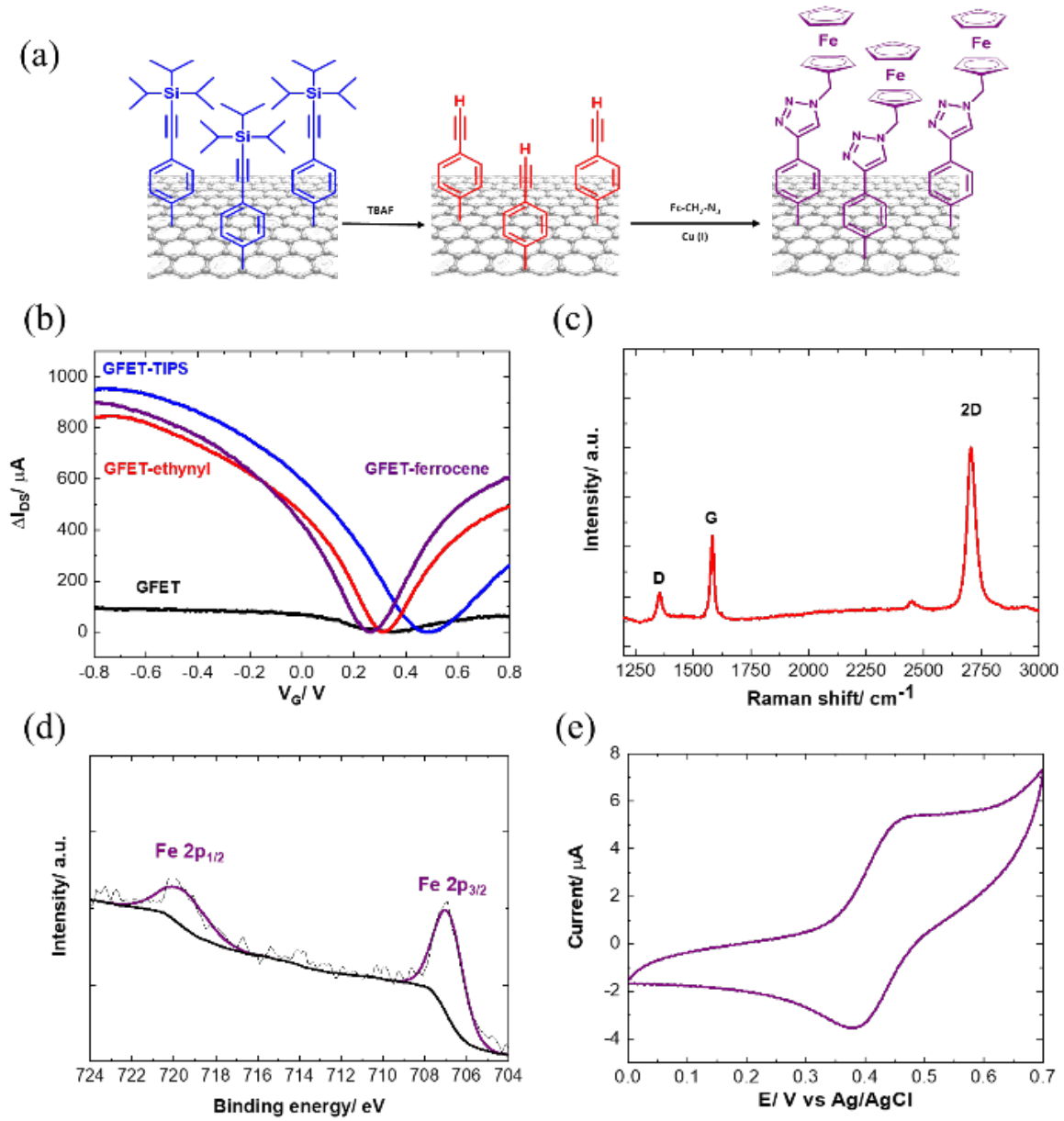

Figure 5. (a) Formation of ethynyl-terminated GFET via deprotection of GFET-TIPS followed by integration of azide-terminated ferrocene through the Cu(I) "click" chemistry approach. (b) $I_{DS}V_G$ of GFET-ethynyl and GFET-ferrocene. (c) Raman spectrum of GFET-ethynyl. (d) High resolution Fe2p XPS core level spectrum of ferrocene-modified GFET interfaces. (e) Cyclic voltammogram of GFET-ferrocene in ethanol/$LiClO_4$ (0.1 M), scan rate = 100 mVs^{-1}.

Figure 5e depicts the cyclic voltammogram of the ferrocene modified electrode examined in an electrolytic ethanol solution. A surface concentration of $\Gamma = 3.8\times10^{-10}$ mol cm^{-2} of bound ferrocene groups was derived from these measurements using the following equation:

$$\Gamma = Q/nFA \quad (3)$$

where Q is the passed charge, n the number of exchanged electrons (n=1), F the Faraday constant and A is the electroactive surface of the electrode determined as 0.10 cm^2. The number of attached ferrocenyl groups here is determined (limited) by the size of the TIPS group which is bulkier than the size of ferrocene.[42] Considering the ferrocene molecules as spheres with a diameter of 6.6 Å, the theoretical maximum coverage for an idealized ferrocene monolayer can be estimated as $\Gamma = 4.4\times10^{-10}$ mol cm^{-2}.[52] In our case, $\Gamma = 3.8\times10^{-10}$ mol cm^{-2} (86%) of the maximum surface coverage is achieved, in good agreement with previous observation and is close to the theoretical maximum coverage value.[43] From the $I_{DS}V_G$ curve of ferrocenyl terminated GFET, it is evident that the charge mobilities are not significantly altered in this surface modification process being $\mu_{h=}$1203 $cm^2V^{-1}s^{-1}$ (initially 1253 $cm^2V^{-1}s^{-1}$ for this device) and $\mu_{e=}$1102 $cm^2V^{-1}s^{-1}$ (initially 1180 $cm^2V^{-1}s^{-1}$ for this device) respectively.

The positive shift of Dirac point is believed to be in correlation with p-doping due to the presence of the electron withdrawing nature of the ferrocenyl group or the triazole linkage of the click chemistry.

The validate the general concept of the interest of ethynyl modified GFETs, different azide-terminated ligand such as N_3-terminated poly(ethylene glycol) (PEG) (N_3-PEG-NH_2, N_3-PEG-COOH and N_3-PEG-Iodoacetyl) as well as an azide-terminated bioreceptors, in our case a tetrahydrocannabinol aptamer (N_3-aptamer), were clicked onto the ethynyl-terminated GFET and the electronic transfer characteristics determined (**Figure S5)**. The charge mobility of graphene modified with the click interfaces is ranging from 839 to 1110 $cm^2V^{-1}s^{-1}$ for holes and 840 to 1056 $cm^2V^{-1}s^{-1}$ for electrons, respectively (**Table S2**). It is therefore demonstrated that the charge transfer characteristics of the modified GFET remain similar even after the covalent attachment of complex biological molecules via Click chemistry coupling reaction.

3. Conclusions

In summary, we covalently functionalized the graphene channel of a graphene-base field effect transistor (GFET) with an ethynylphenyl monolayer in a controlled manner, via the electroreduction of a specifically designed 4-[(triisopropylsilyl)ethynyl]benzene diazonium salt (TIPS-Eth-ArN_2^+). The graphene functionalization requires only one voltammetry cycle to achieve a self-inhibited monolayer coverage. Considering the huge impact of such covalent functionalization on the graphene lattice, the GFET keeps a high charge mobility above 1000

$cm^2V^{-1}s^{-1}$. It largely outperforms GFETs modified with other aryl diazonium salts, such as the well-known 4-nitrobenzene diazonium tetrafluoroborate. The functionalization process furthermore induced *p*-type doping due to the electron-withdrawing properties of the triisopropylsilyl (TIPS) protecting groups. Whereas after TIPS deprotection such *p*-type doping are no more observed, the GFET charge mobility is preserved. Raman spectroscopy data are in line with the finding that the integration of TIPS-Eth-Ar introduces only small defects. Introduction of a wide range of (bio) molecules by Click Chemistry reaction (Huisgen 1,3-dipolar cycloaddition) is therefore possible and evidence here by the immobilization of a monolayer of redox active ferrocenyl moieties. It is also important to note here that the fabrication process of the GFET only involved graphene transfer onto commercially available gold interdigitated electrode (IDE) substrates without the need of any lithography techniques. Such a device is ideally suited for achieving highly sensitive GFET based sensing devices, with symmetric $I_{DS}V_G$ curve and slopes of ~1750 $\mu A/V_G$. We are currently investigating the sensitivity and LOD of such devices as biosensor for sensing of cardiac troponin I. Indeed, cardiovascular diseases result in millions of deaths around the globe, many of which could have been avoided if identified at an early stage. The specific sensing of cTnI on TIPS-modified GFET diagnostics might be a step in this direction, but needs still further considerations, notable clinically relevant sample analysis, out of the scope of this work.

4. Experimental Section

Chemicals: Tetrabutylammonium fluoride (TBAF), 4-bromobenzenediazonium tetrafluoroborate (96 %),4-nitrobenzenediazonium tetrafluoroborate, copper(I) sulfate ($CuSO_4$), L-ascorbic acid, ethylenediaminetetraacetic acid (EDTA), N-butylhexafluorophosphate ($n Bu_4PF_6$) and O-(2-Aminoethyl)-O‘-(2-azidoethyl)heptaethylene glycol (N_3-PEG-NH_2), were purchased from Sigma-Aldrich and used as-received. 4-((triisopropylsilyl)ethylenyl)benzene diazonium tetrafluoroborate (TIPS-Eth-ArN_2^+) and azidomethylferrocene were synthesized as reported previously.[43]

Azido-PEG-acid was purchased from Broadpharm (San Diego, USA) and Iodoacetyl-PEG-Azide was purchased from NanoCS (New York, USA).

5‘-azide modified tetrahydrocannabinol aptamer (5‘-NH2-TTT-TTT-CTT ACG ACC CAG GGG GGT GGA CAG GCG GGG GTT AGG GGG GTC GTA AG-3‘) was purchased from integrated DNA Technologies (Leuven, Belgium).

Materials: Prior to graphene transfer, the interdigitated microelectrodes (ED-IDE1-Au w/o SU8, Micrux Technologies) are cleaned in an UV-Ozone chamber (Jelight, USA) for 10 min followed

by submersion for 15 min sequentially in 10 mL of acetone, isopropanol and water. Finally, every chip is copiously rinsed with large amount of water and dried under a nitrogen flow. The cleaned interfaces are placed in a plastic Petri dish and stored in a desiccator under vacuum. The cleaned IDE are modified with trimethoxyphenylsilane (TMPS, 300 μL of TMPS in 15 mL of ethanol) in a plastic falcon tube for 1 h. Afterwards, the electrodes are immersed for 15 min in ethanol to remove the excess of the silane compounds from the surface. Subsequently, the modified interfaces are nitrogen blow dried and stored under vacuum. The chips are placed on a hot plate at 120 °C at ambient pressure for 2 h to anneal the formed monolayer and provide complete removal of the solvents from the surface. Graphene is directly transferred to these interfaces.

Graphene: The monolayer graphene is grown by chemical vapor deposition (CVD) on commercial Cu foil from Alpha Aesar (high purity - 99.9999%). Graphene growth is carried out in a Jipelec JetFirst Rapid Thermal CVD (RTCVD). This system allows heating and cooling at high rates (10 °C s^{-1}). The growth itself comprises heating, annealing, growth and cooling steps. We used a mixture of 100 sccm of argon and 5 sccm of dihydrogen during all the steps and 20 sccm of methane as a precursor during the growth phase. We first cut the Cu foil in small pieces (2.5 × 2.5 cm), clean them with acetic acid, acetone and IPA for 5min each under ultrasonication in order to remove all possible copper oxide and to produce the cleanest surface possible. We then put the pieces onto a Si wafer in the chamber. We proceed to a high vacuum ($<5 \times 10^{-5}$ bar) before starting and then the sample is heated for 5 min from room temperature to 300 °C, followed by 2 min from 300 °C to 1070 °C, annealing for 5 min, growth for 5 min and finally, a quick cooling of the chamber using a water flow (with a decrease rate of 60 °C s^{-1} from 1000 to 700 °C), for 10 min to reach room temperature.

Transfer: A polymethyl methacrylate (PMMA) film of 200 nm in thickness is spin-coated onto the graphene/Cu foil and annealed at 110 °C with a very slow heating and cooling rate (1 °C min^{-1}) in order to prevent cracks in the graphene due to the difference of the thermal expansion coefficient between copper and graphene. The graphene on the back side of the Cu foil was removed by reactive ion etching (RIE) in an O_2 plasma (50 W/100 mT/25 sccm/1 min). Copper foil etching was achieved in 0.2 M ammonium persulfate ($(NH_4)_2S_2O_8$) for 8 h and the floating PMMA/graphene sample was put in a DI water. This operation was repeated about 10 times in order to rinse the graphene from the etchant solution. Graphene transfer onto the IDE was achieved by submerging the IDE under the floating graphene/PMMA film. To remove traces of trapped water between graphene and IDE and to increase the adhesion of graphene to the IDE, the substrate was placed on a hot plate and annealed at 90 °C for 30 min using a slow

heating and cooling rate (1 °C min^{-1}). The PMMA layer was effectively removed by UV/ozone cleaning at 28-35 mW cm-2 for 5 min followed by a hot acetone rinse (30 °C for 30 min).

Electrografting: The electrografting of 4-((triisopropylsilyl)ethylenyl)benzene diazonium tetrafluoroborate (TIPS-Eth-ArN_2^+) (10 mM) in 0.1 M *n*-tetrabutylhexafluorophosphate (*n*Bu_4PF_6) in acetonitrile was performed using cyclic voltammetry at a scan rate of 50 mV s^{-1} for five cycles between +0.20 V and -0.60 V *vs.* Ag/AgCl. The electrodes were rinsed with copious amounts of acetonitrile and acetone and gently dried under argon.

TIPS Deprotection: TIPS protecting group was removed by the immersion of the interface into tetrabutylammonium fluoride (TBAF, 0.1 M in THF) for 1h at room temperature. The surface was then left for 15 min in a pure THF solution for cleaning. This modification process produces an ethynyl-terminated GFET.

Cu(I)-Catalyzed Click Chemistry: Ethynyl-terminated GFET was immersed into an aqueous solution of $CuSO_4$ (10 mM) and Lascorbic acid (20 mM) in the presence of azidomethylferrocene (0.83 mM in THF) and left for 1 h under argon atmosphere. The interface was then treated with an aqueous solution of EDTA for 10 min to chelate any remaining Cu^{2+} residues and finally washed copiously with acetone and water and left for ambient drying.

Instrumentation: X-ray photoelectron spectroscopy (XPS) was performed on a PHI 5000 VersaProbe-Scanning ESCA Microprobe (ULVAC-PHI, Japan/USA) instrument at a base pressure below 5×10^{-9} mbar. Core level spectra were acquired at pass energy of 23.5 eV with a 0.1 eV energy step. All spectra were acquired with 90º between X-ray source and analyzer and with the use of low energy electrons and low energy argon ions for charge neutralization. After subtraction of the linear background, the core-level spectra were decomposed into their components with mixed Gaussian-Lorentzian (30:70) shape lines using the CasaXPS software. Quantification calculations were conducted using sensitivity factors supplied by PHI. Scanning electron microscopy (SEM) images were obtained using an electron microscope ULTRA 55 (Zeiss, France) equipped with a thermal field emission emitter and three different detectors (EsB detector with filter grid, high efficiency In-lens SE detector and Everhart-Thornley Secondary Electron Detector). Raman spectroscopy measurements were performed on a LabRam HR Micro-Raman system (Horiba Jobin Yvon, France) combined with a 473 nm laser diode as excitation source. Visible light was focused by a 100x objective. The scattered light was collected by the same objective in backscattering configuration, dispersed by an 1800 mm focal length monochromator and detected by a CCD. Raman images in mapping conditions were obtained from a 10 x 10 point array with 2 µm spacing between two consecutive points. Each data point was acquired during 5 s exposure time and is the averaged over three

measurements. The background caused by the gold scattering was corrected against a blank measurement of the clean gold electrode. The images were generated using LabSpec software. Tapping mode AFM images in air and ambient temperate were recorded using a Bruker, Dimension 3100 AFM. The surfaces were imaged with a silicon cantilever (AppNano TM300, typical spring constant: 50 N m^{-1}) working at a frequency of 369 kHz. Image treatment and RMS (root-mean square) roughness Ra were obtained with the WSXM software. Surface roughness of the samples was measured by scanning over a 5 x 5 μm area. Cyclic voltammograms were acquired on a potentiostat/galvanostat (Metrohm Autolab, The Netherlands). Electrical measurements were conducted using a probe station source meter unit U2322A (Keysight Technologies, USA). All measurements were performed using a PMMA commercial flow cell (Micrux Technologies, Spain) with fixed flow channel geometry (16 μL), ensuring a defined flow rate of 50 μL/min to minimize mass transport limitation of the analyte to the sensor surface in all experiments. A silver chloride wire (diameter 1 mm, Sigma-Aldrich) was used to operate the GFET device in liquid gate configuration, with a constant source-drain bias (VDS) of 0.05 V, sweeping the gate voltage (VG) between -0.8 V and 0.8 V.

Supporting Information

Supporting Information is available on the web site

Acknowledgements

Financial support from the Centre National de la Recherche Scientifique (CNRS) and the University of Lille is acknowledged.

References

1. F. Schwierz, *Nat. Nanotechnol.*, 2010, **5**, 487–496.
2. Y. Shao, J. Wang, H. Wu, J. Liu, I. A. Aksay and Y. Lin, *Electrocalaysis*, 2010, **22**, 1027-1036.
3. V. Georgakilas, J. N. Toiwari, C. Kemp, J. A. Perman, A. B. Boulinos, K. S. Kim and R. Zboril, *Chem. Rev.*, 2016, **9**, 5464–5519.
4. J. Park and M. Yan, *Acc. Chem. Res.*, 2013, **46**, 181.
5. C. C.-K. and M. Pumera, *Chem. Soc. Rev.*, 2013, **43**, 3222.
6. K. S. Novoselov, A. K. Geim, S. V. Morozov, D. Jiang, Y. Zhang, S. V. Dubonos, I. V. Grigorieva and A. A. Firsov, *Science*, 2004, **306**, 66.
7. F. Schedin, A. K. Geim, S. V. Morozov, E. W. Hill, P. Blake, M. I. Katsnelson and K. S. Novoselov, *Nat. Mater.*, 2007, **6**, 652-655.
8. J. Lee, E. Hwang, E. Lee, S. Seo and H. Lee, *Chem. Eur. J.*, 2012, **18**, 5155 – 5159.

9. W. Fu, L. Jiang, E. P. van Geest, L. M. C. Lima and G. F. Schneider, *Adv. Mater.*, 207, **29**, 1603610.
10. J. Liu, J. Tang and J. J. Gooding, *J. Mater. Chem.*, 2012, **22**, 12435-12452.
11. A. Lopez and J. Liu, *Adv. Intell. Syst.*, 2020, **2**, 2000123.
12. G. L. C. Paulus, Q. H. Wang and M. S. Strano, *Acc. Chem. Res.*, 2012, **46**, 160–170.
13. G. Ambrosio, A. Brown, L. Daukiya, G. Drera, G. Di Santo, L. Petaccia, S. De Feyter, L. Sangaletti and S. Pagliara, *Nanoscale*, 2020, **12**, 9032-9037
14. D. K. H. Tsang, T. J. Lieberthal, C. Watts, I. E. Dunlop, S. Ramadan, A. E. del Rio Hernandez and N. Klein, *Sci. Rpt.*, 2019, **9**, 13946.
15. E. Beyarova, M. E. Itkis, P. Ramseh, C. Berger, M. Spinkle, W. A. de Heer and R. C. Haddon, *J. Am. Chem. Soc.*, 2009, **131**, 1336-1337.
16. Z. Xia, F. Leonardi, M. Gobbi, Y. Liu, V. Bellani, A. Liscio, A. Kovtun, R. Li, X. Feng, E. Origu, P. Samori, E. Treossi and V. Palermo, *ACS Nano*, 2016, **10**, 7125-7134.
17. C.-J. Shi, Q. H. Wan, Z. Jin, G. L. C. Paulus, D. Blankschtein, P. Jarillo-Herrero and M. S. Strano, *Nano Lett*, 2013, **13**, 809-817.
18. D.-e. Jiang, B. G. Sumpter and S. Dai, *J. Phys. Chem. B*, 2006, **110**, 23628.
19. H. Lim, J. S. Lee, H.-J. Shin, H. S. Shin and H. C. Choi, *Langmuir* 2010, **26**, 12278–12284.
20. Z. Sun, S.-i. Kohama, Z. Zhang, J. R. Lomeda and J. M. Your, *Nano Res* . 2013, **3**, 117–125.
21. F. M. Koheler, A. Jacobus, K. Ensslin, C. Stampfer and W. J. Stark, *Small*, 2010, **6**, 1125– 1130. .
22. R. Sharma, J. H. BAik, C. J. Perera and M. S. Strano, *Nano Lett.*, 2010, **10**, 398–405.
23. X.-Y. Fan, R. Nouchi, L.-C. Yin and K. Tanigaki, *Nanoechnolgy*, 2010, **21**, 475208.
24. E. Pembroke, G. Ruan, A. Stinitskii, D. A. Corley, Z. Yan, Z. Sun and J. M. Your, *Nano Research* 2013, **6**, 138–148.
25. D. Bousa, O. Jankovsky, D. Semidubsky, J. Luxa, J. Strural, M. Pumera and Z. Sofer, *Chem. Eur. J.* , 2015, **21**, 17728 – 17738.
26. D. B. Farmer, R. Goliazadeh-Mojarad, V. Perebeinos, Y.-M. Lin, G. S. Tulevski, J. C. Tsand and P. Avouris, *Nano Lett.*, 2009, **9**, 388-392.
27. X. Dong, Q. Long, A. Wei, W. Zhang, L.-J. Li, P. Chen and W. Huang, *Carbon*, 2012, 1517 –1522.
28. M. Min, S. Seo, J. Lee, S. M. Lee, E. Hwang and H. Lee, *Chem. Commun.*, 2013, **49**, 6289.
29. J. Lu, A. Lipatov, N. S. Vorebeva, D. S. Muratov and A. Sinitskii, *Adv. Electron. Mater.* , 2018, **4**, 1800021. .
30. V. V. Rostovtsev, L. G. Green, V. V. Fokin and K. B. Sharpless, *Angew. Chem., Int. Ed.* , 2002, **41**, 2596.
31. C. W. Tornoe, C. Christensen and M. Meldal, *J. Org. Chem.* , 2002, **67**, 3057.
32. J.-B. Wu, M.-L. Lin, X. Cong, H.-N. Liu and P.-H. Tan, *Chemical Society Reviews*, 2018, **47**, 1822-1873.
33. L. Zhou, L. Fox, M. Wlodek, L. Islas, A. Slastanova, E. Robles, O. Bikondoa, R. Harniman, N. Fox, M. Cattelan and W. H. Briscoe, *Carbon*, 2018, **136**, 255-261.
34. K. I. Bolotin, K. J. Sikes, Z. Jiang, M. Klima, G. Fudenberg, J. Hone, P. Kim and H. L. Stormer, *Solid State Communications*, 2008, **146**, 351-355.
35. S. V. Morozov, K. S. Novoselov, M. I. Katsnelson, F. Schedin, D. C. Elias, J. A. Jaszczak and A. K. Geim, *Physical Review Letters*, 2008, **100**, 016602.
36. W. Fu, L. Jiang, E. P. van Geest, L. M. C. Lima and G. F. Schneider, *Advanced Materials*, 2017, **29**, 1603610.

37. J.-H. Chen, C. Jang, S. Xiao, M. Ishigami and M. S. Fuhrer, *Nature Nanotechnology*, 2008, **3**, 206-209.
38. J. W. Suk, W. H. Lee, J. Lee, H. Chou, R. D. Piner, Y. Hao, D. Akinwande and R. S. Ruoff, *Nano Letters*, 2013, **13**, 1462-1467.
39. A. Béraud, M. Sauvage, C. M. Bazán, M. Tie, A. Bencherif and D. Bouilly, *Analyst*, 2021, **146**, 403-428.
40. T. Ono, Y. Kanai, K. Inoue, Y. Watanabe, S.-i. Nakakita, T. Kawahara, Y. Suzuki and K. Matsumoto, *Nano Letters*, 2019, **19**, 4004-4009.
41. M. Hasegawa, Y. Hirayama, Y. Ohno, K. Maehashi and K. Matsumoto, *Japanese Journal of Applied Physics*, 2014, **53**, 05FD05.
42. Y. R. Leroux and P. Hapiot, *Chem. Mater.*, 2013, **25**, 489-495.
43. Y. R. Leroux, F. Hui, J.-M. Noel, C. Roux and P. Hapiot, *J. Am. Chem. Soc.*, 2010, **132**, 14039-14041.
44. S. Reich and C. Thomsen, *Philos. Trans. R. Soc.*, 2004, **362**, 2271–2288.
45. P. Solís-Fernández, M. A. Bissett, M. Tsuji and H. Ago, *Nanoscale*, 2015, **7**, 3572-3580.
46. P. Huang, H. Zhu, L. Jiang, Y. Zhao and X. Gao, *ACS Nano*, 2011, **5**, 7945–7949.
47. E. Pembroke, G. Ruan, A. Sinitskii, D. A. Corley, Z. Yan, Z. Sun and J. M. Tour, *Nano Research*, 2013, **6**, 138-148.
48. Q. H. Wang, Z. Jin, K. K. Kim, A. J. Hilmer, G. L. C. Paulus, C.-H. Shih, M.-H. Ham, J. D. Sanchez-Yamagishi, K. Watanabe, T. Taniguchi, J. Kong, P. Jarillo-Herrero and M. S. Strano, *Nat. Chem.*, 2012, **4**, 724.
49. A. Das, S. Pisana, B. Chakraborty, S. Piscanec, S. K. Saha, U. V. Waghmare, K. S. Novoselov, H. R. Krishnamurhty, A. K. Geim, A. C. Ferrari and A. K. Sood, *Nat. Nanotechnol.*, 2008, **3**, 210-215.
50. M. M. Lucchese, F. Stavale, E. H. Martins Ferreira, C. Vilani, M. V. O. Moutinho, R. B. Capaz, C. A. Achete and A. Jorio, *Carbon*, 2010, **48**, 1592-1592.
51. M. M. Lucchese, F. Stavale, E. H. Martins Ferreira, M. V. O. Moutinho, R. B. Capaz, C. A. Achete and A. Joria, *Carbon* 2010, **48**, 1592-1597.
52. C. E. D. Chidsey, C. R. Bertozzi, T. M. Putvinski and A. M. Mujsce, *Journal of the American Chemical Society*, 1990, **112**, 4301-4306.
53. A. Sinitskii, A. Dimiev, D. A. Corley, A. A. Fursina, D. V. Kosnkin and J. M. Tour, *ACS Nano*, 2010, **4**, 1949–1954.

ToC figure

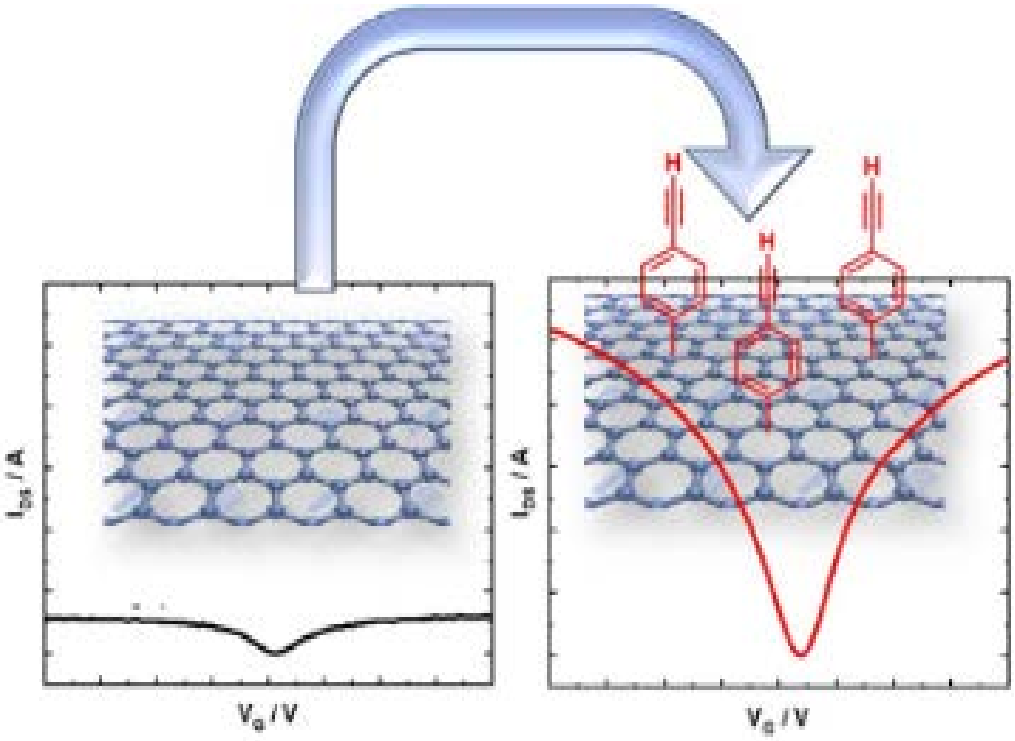

Supporting Information

Controlled Covalent Functionalization of Graphene-Channel of a Field Effect Transistor as Ideal Platform for (Bio)sensing Applications Title

Vladyslav Mishyn, Teresa Rodrigues, Yann R. Leroux, Patrik Aspermair, Henri Happy, Johannes Bintinger, Christoph Kleber, Rabah Boukherroub, Wolfgang Knoll, * and Sabine Szunerits**

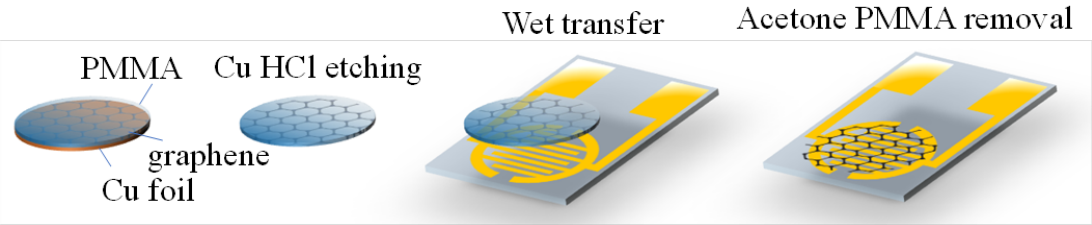

Scheme S1. Process of deposition of CVD graphene on gold-based interdigitated electrodes (IDE). First the backside of the Cu disk is plasma etched to remove the residual graphene, followed by copper foil etching in diluted hydrochloric acid (HCl). The remaining floating graphene sheet, supported by a PMMA layer (60 nm, 495K, A2), is transferred to the IDE chip and annealed for 30 min at 90°C. The PMMA is removed in the final step using a hot acetone washing.

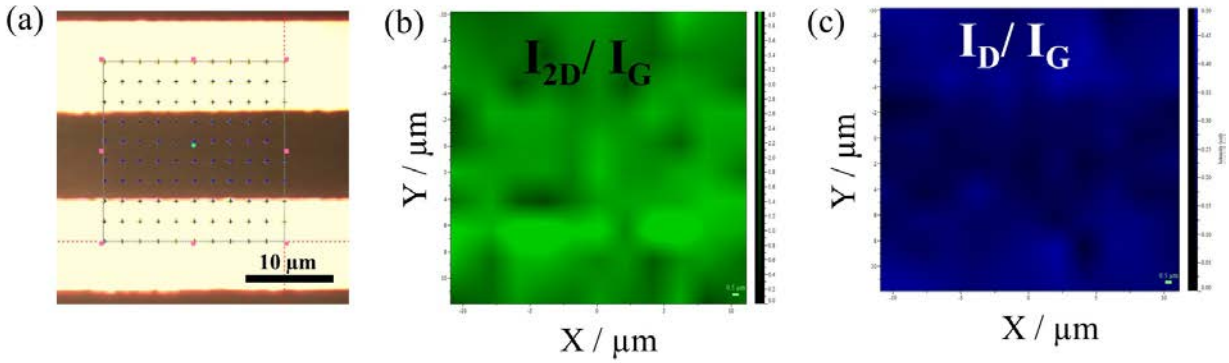

Figure S1. Raman mapping of graphene transferred onto gold based interdigitated electrode (GFET). (a) optical image of the scanned area. (b) I_{2D}/I_G. (c) I_D/I_G.

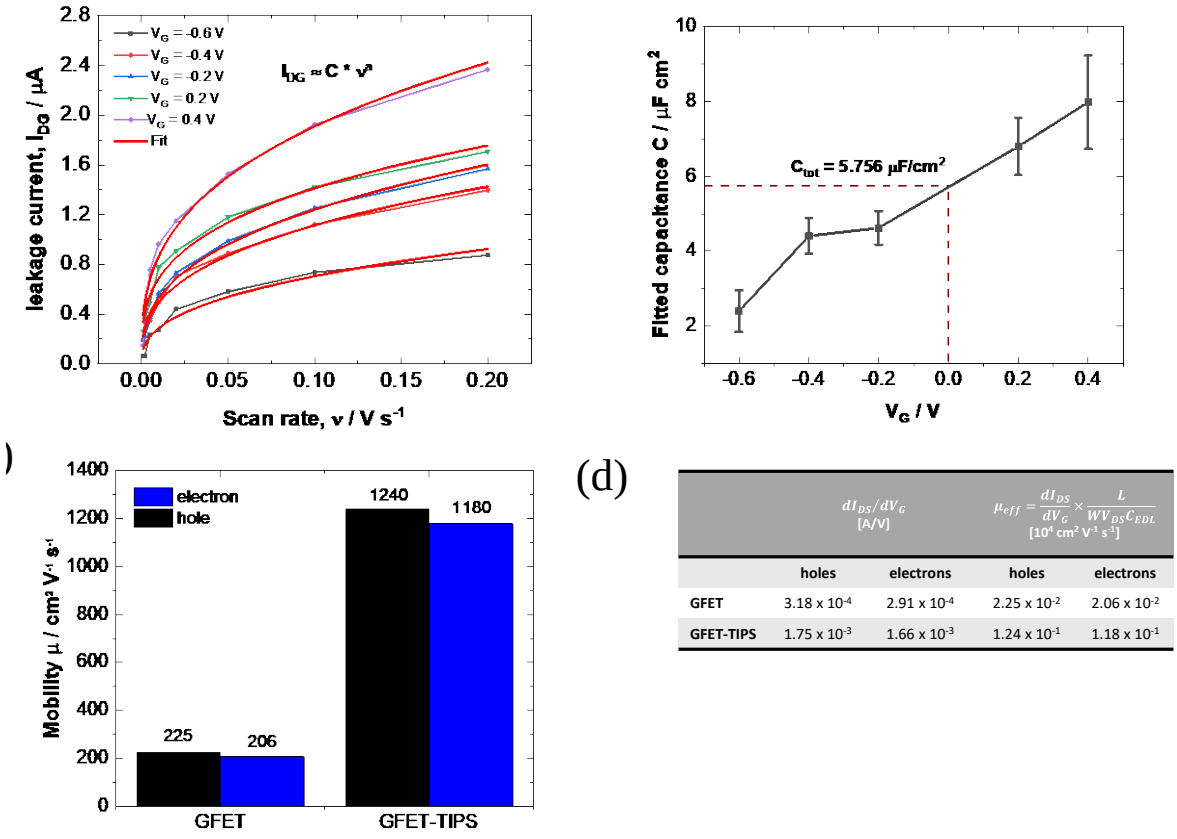

	dI_{DS}/dV_G [A/V]		$\mu_{eff} = \frac{dI_{DS}}{dV_G} \times \frac{L}{WV_{DS}C_{EDL}}$ [10^4 cm^2 V^{-1} s^{-1}]	
	holes	electrons	holes	electrons
GFET	3.18×10^{-4}	2.91×10^{-4}	2.25×10^{-2}	2.06×10^{-2}
GFET-TIPS	1.75×10^{-3}	1.66×10^{-3}	1.24×10^{-1}	1.18×10^{-1}

Figure S2. Determination of hole and electron mobility: (a) Leakage current vs. scan rate recorded at different applied VG. (b) Fitted capacitance vs. VG. (c) Electron and hole mobility of GFET and TIPS modified GFET. (d) Table summarizing hole and electron mobility values for GFET and GF

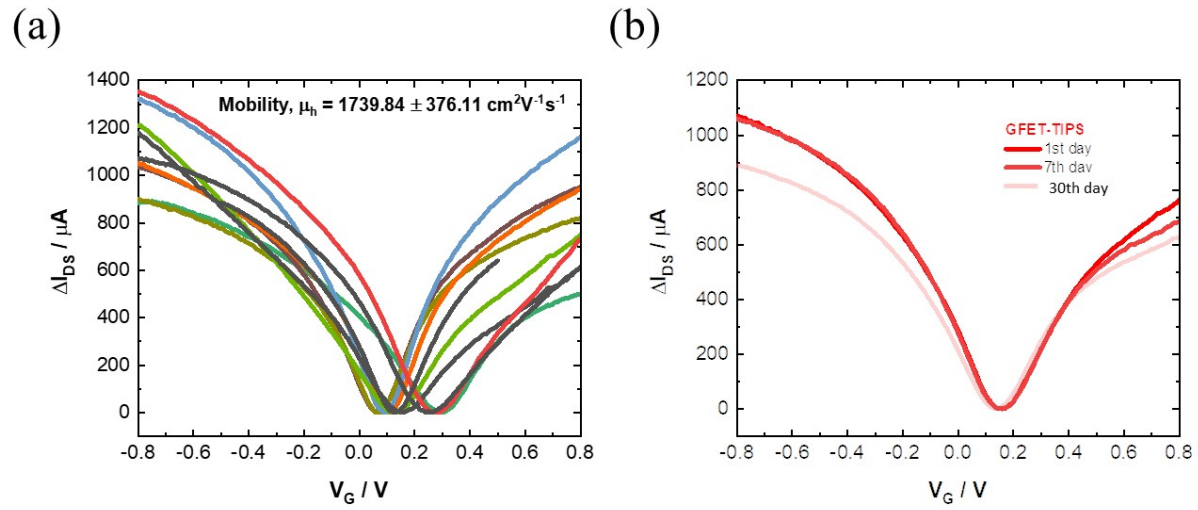

Figure S3. (a) $I_{DS}V_G$ curves of 10 TIPS modified GFET with calculated mobility. (b) Stability of 10 TIPS modified GFETs evaluated after 1 month when stored at room temperature in the dark.

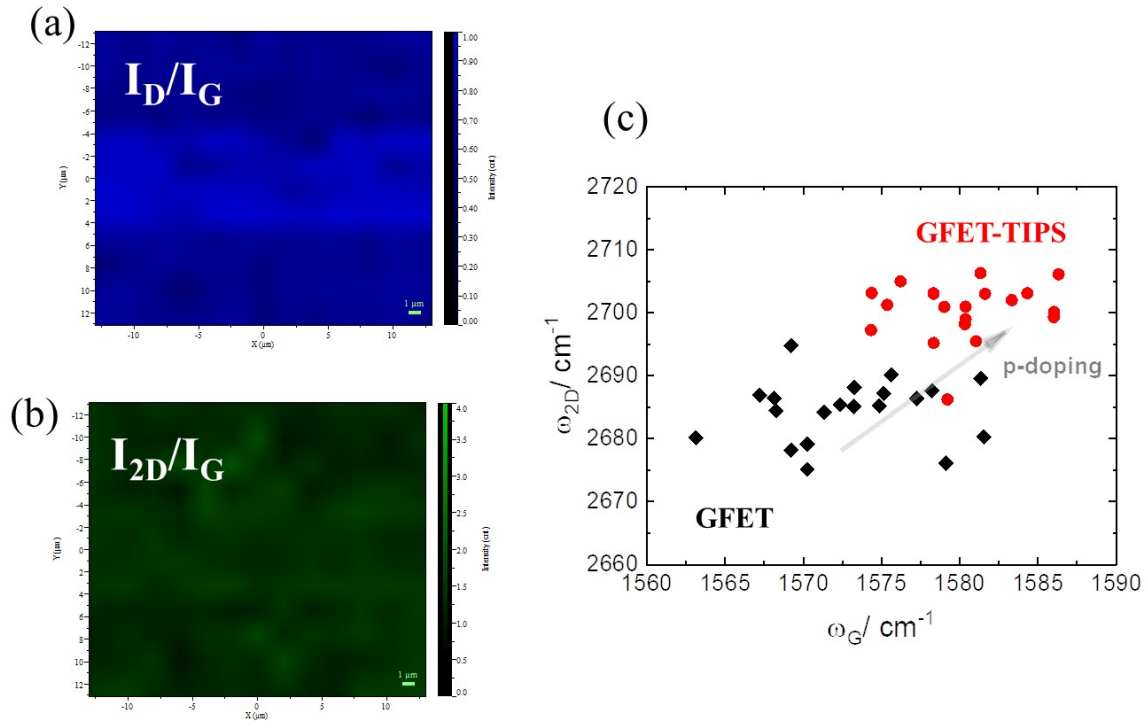

Figure S4. Raman spectroscopy analysis of GFET-TIPS. (a) I_D/I_G. (b) I_{2D}/I_G. (c) Scatter plot of 2D peak position vs. G peak position for GFET, (black, extracted from **Figure S2**) and for GFET-TIPS (red)

(a)

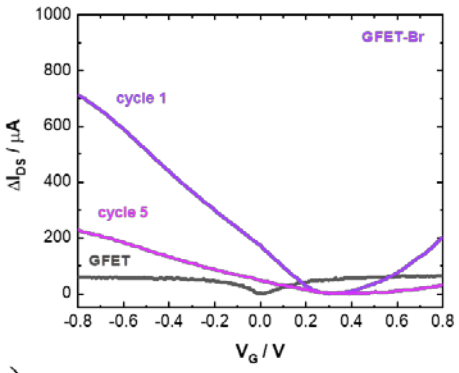

(b)

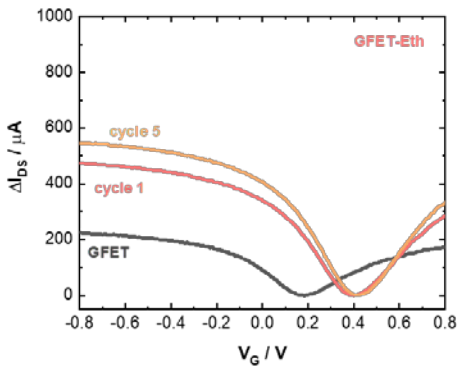

(c)

		Mobility [10^4 cm^2 V^{-1} s^{-1}]	
		Holes	Electrons
4-Eth-Ph-N_2^+	initital	335±70	318
	1st cycle	827±32	587±23
	5th cycle	893±20	587±12
4-Br-Ph-N2$^+$	1st cycle	498±22	176±14
	5th cycle	107±12	35±8
4-NO_2-Ph-N_2^+	1st cycle	826±18	455±12
	5th cycle	451±15	177±14

Figure S4. $I_{DS}V_G$ curves of GFETs before and after modification for one or five cycles with different diazonium salts (a) 4-bromobenzene diazonium tetrafluororate (4-Br-Ph-N_2^+). (b) 4-ethynylphenyl diazonium '4-Eth-Ph-N_2^+). (c) Table of hole and electron mobilities extracted from Figure S4a-c and Figure 4.

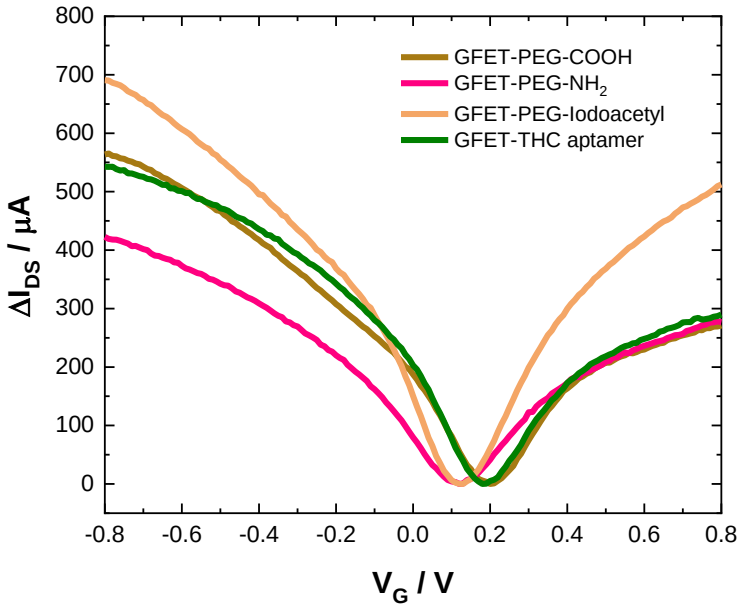

Figure S5: Transfer characteristics of GET-TIPS interfaces modified by click chemistry with different azide-terminated ligands such as azido-PEG-acid (brown), azido-PEG-NH_2 (pink), iodoacetyl-PEG-azide (orange)and a 5'-azide modified tetrahydrocannabinol aptamer (5'-NH_2-TTT-TTT-CTT ACG ACC CAG GGG GGT GGA CAG GCG GGG GTT AGG GGG GTC GTA AG-3') (green)

Table S1: Mobility values of diazonium-modified graphene

Diazonium[a]	Technique	Mobility [$cm^2V^{-1}s^{-1}$]	Ref.
4-NO_2-Ph-N_2^+	Spontaneous grafting	600	23
4-amino-3'-nitroazobenzene diazonium	Spontaneous grafting	580 (hole mobility)	53
4-NO_2-Ph-N_2^+ 4-Me_2N-Ph-N_2^+ 4-CO_2Me-Ph-N_2^+	Spontaneous grafting	500-100 (hole mobility)	24
4-NO_2-Ph-N_2^+	Spontaneous grafting	370 (hole mobility)	46
4-NO_2-Ph-N_2^+ 4-Br-Ph-N_2^+	Electrografting	10	17
4-NO_2-Ph-N_2^+ 4-Br-Ph-N_2^+ 4-Eth-Ph-N_2^+	Electrografting (5 cycles)	451±15 107±12 893±20	Our work

4-TIPS-Eth-Ph-N_2^+		1739± 376	

[a] 4-NO_2-Ph-N_2^+ = 4-nitrobenzene diazonium, 4-Br-Ph-N_2^+ = 4-bromobenzene diazonium, 4-Me_2N-Ph-N_2^+ = 4-dimethylaminobenzene diazonium, 4-CO_2Me-Ph-N_2^+ = 4-methylbenzoate diazonium, 4-Eth-Ph-N_2^+ = 4-ethynylphenyl diazonium, 4-TIPS-Eth-Ph-N_2^+ = 4-triisopropylsilylethynylphenyl diazonium.

Table S2: Mobility values of graphene characteristics before and after interfaces click chemistry

Interface	Hole mobility [$cm^2V^{-1}s^{-1}$]	Electron mobility [$cm^2V^{-1}s^{-1}$]
N_3-PEG-COOH	978±23	1025±51
N_3-PEH-NH_2	839±16	840±51
N_3-PEG-Iodoacetyl	1110±75	1025±54
N_3-THC aptamer	1076±85	1056±34